Image potential states in graphene

V. M. Silkin,[1,2,3] J. Zhao,[4] F. Guinea,[5] E. V. Chulkov,[1,2] P. M. Echenique,[1,2] and H. Petek[2,3,4]

[1]*Depto. de Física de Materiales and Centro Mixto CSIC-UPV/EHU, Facultad de Ciencias Químicas, Universidad del País Vasco, Apdo. 1072, 20080 San Sebastián/Donostia, Spain*

[2]*Donostia International Physics Center (DIPC), P. Manuel de Lardizabal 4, 20018 San Sebastián/Donostia, Spain*

[3]*IKERBASQUE, Basque Foundation for Science, 48011 Bilbao, Spain*

[4]*Department of Physics and Astronomy, Petersen Institute of Nanoscience and Engineering, University of Pittsburgh, Pittsburgh, Pennsylvania 15260, USA*

[5]*Instituto de Ciencia de Materiales de Madrid (CSIC), Sor Juana Inés de la Cruz 3, 28049 Madrid, Spain*

(Received 20 August 2009; published 28 September 2009)

Using combined "LDA+image potential" calculations we show that below the vacuum level a single graphene layer possesses a double Rydberg series of even (n^+) and odd (n^-) symmetry image-potential states and argue that the widely discussed interlayer band in graphite is a consequence of the intersheet hybridization of the first even image-potential state. In light of the present results, the unoccupied electronic states with nearly-free-electron properties in carbon nanotubes, fullerenes, and fullerites can be understood to originate from the image-potential states of graphene.

Carbon is a very versatile element. In nature it can be found in many allotropic forms, and in many of them, such as graphite, fullerenes, and nanotubes, the carbon atoms form strong covalent bonds through hybridization of sp^2 orbitals between three nearest neighbors in a planar or nearly planar configuration. The simplest lattice where this arrangement is found is graphene, a one-atom-thick carbon sheet where the atoms form a honeycomb lattice. The recent isolation of single graphene layers,[1] and the modulation of the carrier concentration within them[2] has stimulated much interest in the electronic properties of graphene and related compounds.[3]

Most ongoing experimental and theoretical work on graphene has focused on its electronic band structure in the vicinity of the $\bar{K}$ point of the two-dimensional Brillouin zone. The electronic bands crossing the Fermi level at the $\bar{K}$ point have remarkable linear energy dispersion, which imparts novel physical phenomena. These bands can be described within a parameterized tight-binding scheme, which, however, is inadequate for the description of the unoccupied part of the energy spectrum. There have also been some calculations at the local-density approximation level,[4–7] but the detailed analysis of graphene electronic structure in the vicinity of the vacuum level, to the best of our knowledge, is lacking.

In the unoccupied spectrum of graphite, the most interesting and extensively studied has been the so-called interlayer state, which is characterized by singularly strong three-dimensional dispersion. As its name suggests, the interlayer state has a charge-density maximum between the basal carbon planes with interlayer dispersion in the 4–7.5 eV range above the Fermi level, and nearly-free-electron-like dispersion parallel to them.[5,8,9] The interlayer state has been observed experimentally by inverse photoemission,[9] inelastic electron scattering,[10] and near-edge x-ray absorption fine structure.[11,12] In a metal-atom-intercalated graphite, the occupation of the band formed by hybridization between the s states of metal ions and the spatially overlapping interlayer state is thought to impart superconducting properties.[13] The

interlayer state has been predicted for multiwall nanotubes, and even for the inner space of single wall nanotubes and fullerenes.[14] Recently, atomiclike unoccupied orbitals of C_{60} molecules discovered by low-temperature scanning tunneling microscopy[15] (STM) were attributed to the same physical origin, the internal exchange-correlation potential of a hollow molecule. Other layered materials also possess similar interlayer states, which in the case of hexagonal BN (Ref. 16) corresponds to the conduction-band minimum. Paradoxically, there is experimental[12] and theoretical[4] evidence that the parent of the interlayer state exists even for a single sheet of graphene.

In order to establish the physical origin of the interlayer state of graphene and related materials we perform *ab initio* calculations of the graphene electronic structure. Present calculations show that the origin of the previously discussed interlayer state of graphene is the lowest-energy member of a double Rydberg series of even and odd image-potential states converging to the vacuum level. Related image-potential states are well known for the semi-infinite metal/vacuum interface,[17] and have been observed for pyrolytic graphite[18] and metal supported nanographene.[19] We further argue that the interlayer state in graphite forms through the intersheet hybridization of the lowest image-potential state in graphene in a similar fashion as in the case of graphene bilayer.[4] The universal properties of the image potential suggest that the strongly dispersing interlayer states are a common property of layered materials.

For calculation of the electronic structure of an isolated graphene we used a repeated-slab geometry with graphene layers separated by large vacuum intervals. Hence the unit cell of the system contains two carbon atoms with lateral and perpendicular lattice constants of 2.434 and 85 Å, respectively, which is sufficient for the convergence of the six lowest-energy image-potential states. Self-consistent density-functional calculations were performed using the plane-wave basis set with a cutoff of 60 Ry and a $72 \times 72 \times 1$ k grid for the density within a local-density approximation (LDA) for exchange-correlation potential.[20] The electron-ion interaction
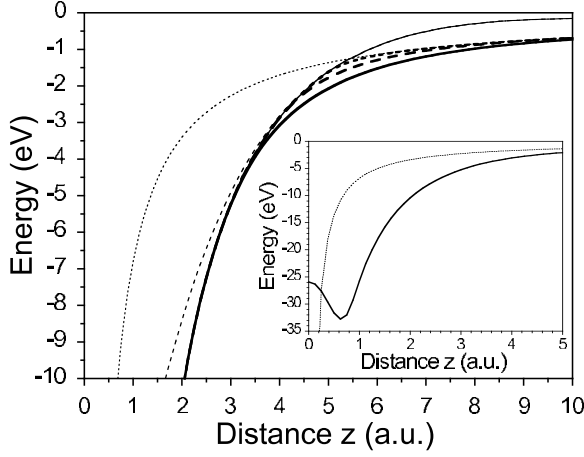
FIG. 1. Averaged in the (x,y) dimensions the local part of the LDA potential (thin solid line) of graphene versus the distance z from the carbon-atom plane. The LDA exchange-correlation potential $V_{xc}(z)$ is shown by the thin dashed line. The thin dotted line shows the image potential $V_{im}(z) = -1/4z$. The thick solid, dashed, and dotted lines show the modified "LDA+image tail" potential $V^M(z)$ constructed with the use of $z_o = 3$, 4, and 5 a.u., respectively. Insert presents $V^M(z)$ with $z_o = 3$ a.u. (solid line) in comparison with $V_{im}(z)$ (dotted line) at the enhanced energy scale. The energies are relative to the vacuum level.

was described by a norm-conserving pseudopotential.[21] Whereas LDA calculations, provide fairly accurate description of bulk and short-range surface potentials, they fail to reproduce the Coulomb-like image-potential tail outside the crystal.[22] Without the correct asymptotic form, this potential cannot predict accurately a Rydberg series of image-potential states. To overcome this problem we use an approach previously employed in the study of image-potential states at metal surfaces.[23] Adopted to the present system, it implies the construction of a hybrid potential which coincides with the self-consistent LDA one at $|z| < z_o$ (the carbon-atom plane is placed at $z = 0$) and at $|z| > z_o$ takes the form valid also for 2D systems[24]

$$V(z) = -\frac{1 - A \cdot e^{-\lambda \cdot |z - \text{sgn}(z) \cdot z_{im}|}}{4|z - \text{sgn}(z) \cdot z_{im}|}. \tag{1}$$

The parameters A and λ are determined from the conditions: (i) $V(z)|_{z=z_o} = V_{xc}(z)|_{z=z_o}$ and (ii) $dV(z)/dz|_{z=z_o} = dV_{xc}(z)/dz|_{z=z_o}$, where $V_{xc}(z) \equiv \frac{1}{S}\int_S V_{xc}(x,y,z)dxdy$, V_{xc} being the LDA self-consistent exchange-correlation potential. To fix the other two parameters, the image plane position z_{im} and z_o, we need more constraints. A free standing graphene sheet has two equivalent surfaces and therefore we put $z_{im} = 0$. Constructed potentials for some values of z_o are shown in Fig. 1 along with the LDA and bare image potentials. We evaluated how the results depend on the position of the matching point z_o. In Table I we report the energies of the lowest-energy unoccupied states at $\bar{\Gamma}$ with respect to the Fermi and the vacuum levels. We assign these states as even and odd image-potential states $n^\pm$, where the signs "+" and "−" refer to their parity with respect to reflection in the

TABLE I. Energy positions of the image-potential states in graphene vs the matching point position, z_o. For each z_o value the energies in first (second) row are given in eV with respect to the Fermi (vacuum) level. Last two lines present the energy values obtained in the LDA calculation (Ref. 37).

z_o (a.u.)	1^+	1^-	2^+	2^-	3^+	3^-
3	2.94	3.69	4.16	4.22	4.30	4.34
	−1.47	−0.72	−0.25	−0.19	−0.11	−0.07
4	3.08	3.80	4.17	4.23	4.30	4.35
	−1.33	−0.61	−0.24	−0.18	−0.11	−0.06
5	3.12	3.84	4.17	4.24	4.30	4.35
	−1.29	−0.57	−0.24	−0.17	−0.11	−0.06
LDA	3.24	4.16	4.29	4.32	4.34	4.40
	−1.17	−0.25	−0.12	−0.09	−0.07	−0.01

graphene plane, and n corresponds to the number of nodes in their wave functions on each side above and below the graphene plane. From Table I it is clear that the energies of these states are sensitive to the shape of the electronic potential at a distance of a few angstroms from the carbon sheet. The potential could be further refined by an experimental determination of these energies. We do not include in the calculations a substrate, which can modify the results, mostly on the substrate side. The effect of a substrate can be incorporated in Eq. (1) through its dielectric constant.

Figure 2 presents the energy spectra evaluated with use of the hybrid "LDA+image-tail" potential constructed for $z_o = 3$ a.u. With the vacuum region size employed we were able to obtain at the $\bar{\Gamma}$ point below the vacuum level up to three members of each infinite series of image-potential states
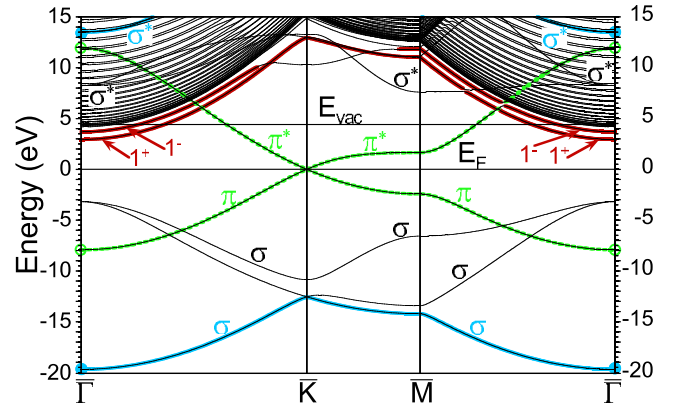

FIG. 2. (Color online) Graphene band structure evaluated with the use of a modified "LDA+image tail" potential constructed for $z_o = 3$ a.u. The bonding and antibonding carbon σ and π states are marked by corresponding symbols. Lowest image-potential states with $n = 1$ are highlighted by thick red (dark gray) lines. The carbon $\sigma(\pi)$ bands that delimit energy gap for the even and odd image-potential states are highlighted by solid blue (light gray) and dashed green (light gray) lines, respectively. Filled and empty circles delimit the corresponding gaps at the $\bar{\Gamma}$ point.
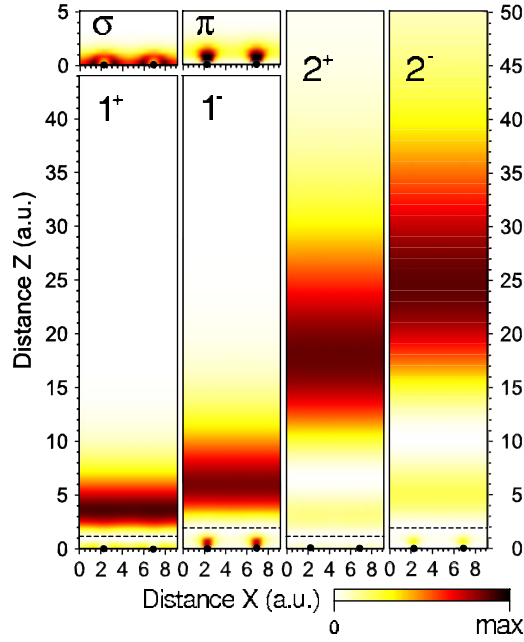
FIG. 3. (Color online) Charge density distribution for 1^+, 1^-, 2^+, and 2^- image-potential states at the $\bar{\Gamma}$ point in the $(10\bar{1}0)$ plane. Dots show carbon atoms positions. Dashed horizontal lines show the first node position of the wave functions. For comparison, on upper-left side the charge densities for the carbon-localized σ and π states are presented.

$$E_n^{\pm} = -0.85 \ \text{eV}/(n + a_n^{\pm})^2, \qquad (2)$$

where $n = 1, 2, 3, \ldots$ is the quantum number of a series member and $a_n^{\pm}$ is the corresponding quantum defect. The higher-energy states are shifted above the vacuum level, as seen in Fig. 2, due to an artificial confinement imposed by the super-cell geometry. In Fig. 2 one can see that below E_{vac} there are no unoccupied carbon $2s$ or $2p$ orbital-derived bands in the vicinity of the $\bar{\Gamma}$ point. The closest occupied σ and unoccupied σ^* carbon $2p_x, 2p_y$ orbital-derived bands with energies at $\bar{\Gamma}$ of -3.2 and $+8.3$ eV, respectively, can be connected with the similar bands in graphite. Their charge densities are confined very close to the carbon sheet and therefore are only slightly modified when the graphite crystal is formed. Their negligible dispersion[25] in graphite along the perpendicular direction confirms this point. Because of their symmetry these states have no effect on the image-potential states around the $\bar{\Gamma}$ point. Indeed, the even and odd image-potential states experience different energy gaps in the band structure of graphene. The relevant energy gaps at $\bar{\Gamma}$ are between the carbon $2s(2p_z)$ orbital-derived $\sigma(\pi)$ states at -19.7 (-7.8) and $+13.5$ eV $(+11.9$ eV$)$ [shown by filled (empty) circles in Fig. 2] for the even (odd) image-potential states. Hence the two image-potential states series are aligned differently within their respective energy gaps.

The extent of interaction of the even- and odd-symmetry image-potential states with the σ and π bands is also reflected in different positions of their wave-function maxima and nodes with respect to the carbon plane, as seen in Fig. 3.

For the even image-potential states the first maximum coincides with that of the σ electron density at the molecular plane, while for the odd ones the first maxima strongly overlap with the π-electron density. The first nodes of even and odd states, respectively, appear at $z_{node} \approx 1$ a.u. and $z_{node} \approx 2$ a.u. corresponding to the falling tails of the σ and π-electron densities. The probability densities of even and odd image-potential states presented in Fig. 3, correlate with the corresponding electron density of the occupied σ and π carbon-derived states as required by the wave-function orthogonality. With increasing of quantum number n the energy splitting between even and odd states with the same n rapidly decreases in accord with decreasing of amplitude of the corresponding wave functions in the carbon sheet region (e.g., compare the charge densities for the $1^{\pm}$ and $2^{\pm}$ states in Fig. 3).

Analyzing the charge-density distribution of the image-potential states presented in Fig. 3 one can see that the maximum for the 1^+ state is located at $z \approx 3.5$ a.u., i.e., close to the middle of the interlayer spacing in graphite. Therefore, assembling graphene layers to form a graphite crystal will affect this state the least, as compared with the higher-energy image-potential state wave functions which extend further into the vacuum. In light of this, the widely discussed interlayer band in graphite can be considered a progeny of hybridization of the 1^+ graphene image-potential states between the adjacent carbon layers. The higher n members of this family are shifted to significantly higher energies when the graphite is formed. For hollow carbon structures derived from graphene, the exchange-correlation potential that to a large extent defines the properties of the 1^+ state, also gives rise to the nearly-free-electron states of nanotubes,[26] and superatom states of fullerenes.[14,15]

The present results show the range of energies available for the image-potential states localized outside the graphene layer. Because of the bilateral symmetry and confinement of the graphene sheet these states in graphene are more strongly bound in comparison with semi-infinite systems. Supporting graphene sheet on a substrate will shift these states toward higher energies and make them more delocalized on the vacuum side. It is known that both suspended graphene layers and layers on a substrate are corrugated,[27,28] with height variations on the order of a few nanometers over scales of 20–50 nm. In this case the odd-even symmetry will be broken and the concave surface states will be stabilized with respect to the convex.[12] Finally, the image potential can be modified by an applied gate voltage sufficiently close to the layer[24,29–31] or by the electric field induced by an STM tip.[28,32,33]

The following picture can be gleaned from the present results. The electronic structure of graphene can be analyzed into carbon-valence-orbital-derived tightly localized σ and π states, and in addition extended unoccupied states that primarily exist in the vacuum above and below the graphene plane. For the building block of graphitic materials, graphene, we identify for the first time the dual Rydberg-like series of these even- and odd-symmetry states. When graphene layers are assembled into a graphite crystal, the interlayer band can be viewed as a consequence of trapping and hybridization of the lowest-energy 1^+ image-potential

state. Moreover, the unoccupied electronic states in other carbon-based nanostructures, like fullerenes,[15] fullerites,[14] and nanotubes[34–36] can be understood as having the common origin with the graphene image-potential states found in the present work. A large extent of wave functions of the image-potential states in the vacuum implies that they are very sensitive to any change of shape or/and environment of the graphene sheet. Hence the image-potential states of graphene and the nearly-free-electron states of graphitic materials derived from them present attractive objects for investigation of how the topography, intersheet and impurity interactions etc., affect their spectroscopic and dynamical properties.

[1] K. S. Novoselov, A. K. Geim, S. V. Morozov, D. Jiang, Y. Zhang, S. V. Dubonos, I. V. Grigorieva, and A. A. Firsov, Science **306**, 666 (2004).

[2] K. S. Novoselov, D. Jiang, F. Schedin, T. J. Booth, V. V. Khotkevich, S. V. Morozov, and A. K. Geim, Proc. Natl. Acad. Sci. U.S.A. **102**, 10451 (2005).

[3] A. H. Castro Neto, F. Guinea, N. M. R. Peres, K. S. Novoselov, and A. K. Geim, Rev. Mod. Phys. **81**, 109 (2009).

[4] M. Posternak, A. Baldereschi, A. J. Freeman, E. Wimmer, and M. Weinert, Phys. Rev. Lett. **50**, 761 (1983).

[5] M. Posternak, A. Baldereschi, A. J. Freeman, and E. Wimmer, Phys. Rev. Lett. **52**, 863 (1984).

[6] S. B. Trickey, F. Müller-Plathe, G. H. F. Diercksen, and J. C. Boettger, Phys. Rev. B **45**, 4460 (1992).

[7] T. O. Wehling, I. Grigorenko, A. I. Lichtenstein, and A. V. Balatsky, Phys. Rev. Lett. **101**, 216803 (2008).

[8] N. A. W. Holzwarth, S. G. Louie, and S. Rabii, Phys. Rev. B **26**, 5382 (1982).

[9] Th. Fauster, F. J. Himpsel, J. E. Fischer, and E. W. Plummer, Phys. Rev. Lett. **51**, 430 (1983).

[10] V. N. Strocov, P. Blaha, H. I. Starnberg, M. Rohlfing, R. Claessen, J.-M. Debever, and J.-M. Themlin, Phys. Rev. B **61**, 4994 (2000).

[11] D. A. Fischer, R. M. Wentzcovitch, R. G. Carr, A. Continenza, and A. J. Freeman, Phys. Rev. B **44**, 1427 (1991).

[12] D. Pacilé, M. Papagno, A. Fraile Rodríguez, M. Grioni, L. Papagno, Ç. Ö. Girit, J. C. Meyer, G. E. Begtrup, and A. Zettl, Phys. Rev. Lett. **101**, 066806 (2008).

[13] G. Csányi, P. B. Littlewood, A. H. Nevidomskyy, C. J. Pickard, and B. D. Simons, Nat. Phys. **1**, 42 (2005).

[14] J. Zhao, M. Feng, J. Yang, and H. Petek, ACS Nano **3**, 853 (2009).

[15] M. Feng, J. Zhao, and H. Petek, Science **320**, 359 (2008).

[16] X. Blase, A. Rubio, S. G. Louie, and M. L. Cohen, Phys. Rev. B **51**, 6868 (1995).

[17] P. M. Echenique and J. B. Pendry, J. Phys.: Condens. Matter **11**, 2065 (1978).

[18] J. Lehmann, M. Merschdorf, A. Thon, S. Voll, and W. Pfeiffer, Phys. Rev. B **60**, 17037 (1999).

[19] I. Kinoshita, D. Ino, K. Nagata, K. Watanabe, N. Takagi, and Y. Matsumoto, Phys. Rev. B **65**, 241402(R) (2002).

[20] D. M. Ceperley and B. J. Alder, Phys. Rev. Lett. **45**, 566 (1980); as parametrized by J. P. Perdew and A. Zunger, Phys. Rev. B **23**, 5048 (1981).

[21] N. Troullier and J. L. Martins, Phys. Rev. B **43**, 1993 (1991).

[22] N. D. Lang and W. Kohn, Phys. Rev. B **1**, 4555 (1970).

[23] V. M. Silkin, E. V. Chulkov, and P. M. Echenique, Phys. Rev. B **60**, 7820 (1999).

[24] G. Gumbs, D. Huang, and P. M. Echenique, Phys. Rev. B **79**, 035410 (2009).

[25] J. C. Boettger, Phys. Rev. B **55**, 11202 (1997).

[26] E. R. Margine and V. H. Crespi, Phys. Rev. Lett. **96**, 196803 (2006).

[27] J. C. Meyer, A. K. Geim, M. I. Katsnelson, K. S. Novoselov, T. J. Booth, and S. Roth, Nature (London) **446**, 60 (2007).

[28] E. Stolyarova, K. T. Rim, S.-M. Ryu, J. Maulzsch, P. Kim, L. E. Brus, T. F. Heinz, M. S. Hybertsen, and G. W. Flynn, Proc. Natl. Acad. Sci. U.S.A. **104**, 9209 (2007).

[29] G. Liu, J. Velasco, Jr., W. Bao, and C. N. Lau, Appl. Phys. Lett. **92**, 203103 (2008).

[30] R. V. Gorbachev, A. S. Mayorov, A. K. Savchenko, D. W. Horsell, and F. Guinea, Nano Lett. **8**, 1995 (2008).

[31] A. F. Young and P. Kim, Nat. Phys. **5**, 222 (2009).

[32] V. Geringer, M. Liebmann, T. Echtermeyer, S. Runte, M. Schmidt, R. Rückamp, M. C. Lemme, and M. Morgenstern, Phys. Rev. Lett. **102**, 076102 (2009).

[33] A. L. Vázquez de Parga, F. Calleja, B. Borca, M. C. G. Passeggi, Jr., J. J. Hinarejos, F. Guinea, and R. Miranda, Phys. Rev. Lett. **100**, 056807 (2008).

[34] B. E. Granger, P. Král, H. R. Sadeghpour, and M. Shapiro, Phys. Rev. Lett. **89**, 135506 (2002).

[35] M. Zamkov, H. S. Chakraborty, A. Habib, N. Woody, U. Thumm, and P. Richard, Phys. Rev. B **70**, 115419 (2004).

[36] M. Zamkov, N. Woody, B. Shan, H. S. Chakraborty, Z. Chang, U. Thumm, and P. Richard, Phys. Rev. Lett. **93**, 156803 (2004).

[37] Note that in *ab initio* LDA calculations the lowest image-potential-like states can be obtained below the vacuum level (as it is in the present case) due to residual unavoidable LDA charge density at the vacuum side preventing vanishing of V_{xc}. In this case their energies are determined by the size of vacuum space used.